Gas– Solid Turbulent Flow in a Circulating Fluidized Bed Riser: Experimental and Numerical Study of Monodisperse Particle Systems

ARTICLE *in* INDUSTRIAL & ENGINEERING CHEMISTRY RESEARCH · SEPTEMBER 2009

Impact Factor: 2.59 · DOI: 10.1021/ie8015285

5 AUTHORS, INCLUDING:

Niels G Deen
Technische Universiteit Eindhoven
175 PUBLICATIONS **3,006** CITATIONS
SEE PROFILE

M. Van Sint Annaland
Technische Universiteit Eindhoven
273 PUBLICATIONS **5,713** CITATIONS
SEE PROFILE

Hans A. M. Kuipers
Technische Universiteit Eindhoven
436 PUBLICATIONS **9,478** CITATIONS
SEE PROFILE

Gas−Solid Turbulent Flow in a Circulating Fluidized Bed Riser: Experimental and Numerical Study of Monodisperse Particle Systems

Y. He,[†,‡] N. G. Deen,*[,†] M. van Sint Annaland,[†] and J. A. M. Kuipers[†]

Faculty of Science and Technology, Institute of Mechanics, Processes and Control Twente (IMPACT), University of Twente, P.O. Box 217, NL-7500 AE Enschede, The Netherlands, and Department of Power Engineering, College of Energy Science and Engineering, Harbin Institute of Technology, Harbin 150001, China

Hydrodynamics of gas-particle two-phase turbulent flow in a circulating fluidized bed riser is studied experimentally by particle image velocimetry (PIV) and numerically with the use of a 3D discrete hard sphere particle model (DPM). The influence of the superficial gas velocity and the solids flux on the flow patterns at different vertical positions has been investigated. Mean particle velocities and rms velocities are obtained, and the influence of turbulence on the flow is investigated. It was found that the superficial gas velocity has a strong influence on the vertical solids velocity but only a minor influence on the extent of solids downflow. The solids flux has a large effect on the extent of solids downflow but only little influence on the lateral profile of the rms vertical solids velocity. The experimental data are analyzed and compared with the numerical results showing a reasonable agreement.

1. Introduction

Gas−solid fluidization using circulating fluidized beds has found widespread application in industry, e.g. in fluid catalytic cracking (FCC) and CFB combustors. However, the behavior of complex flow structures emerging in this type of turbulent two-phase flow is still not fully understood, despite their importance on the overall reactor performance. Detailed experimental and numerical techniques are required to study the flow structures pertaining in CFB reactors in detail.

Some researchers have carried out experimental work to study the flow phenomena in circulating fluidized beds.[1−18] Most of them apply phase Doppler anemometry (PDA) or laser Doppler anemometry (LDA) to measure the flow characteristics in the riser. Laser Doppler anemometry (LDA) is a point measurement technique that is very well suited to measure the velocity and turbulence distribution in both free flows and internal flows at a high temporal resolution. Phase Doppler anemometry (PDA) is a similar technique that enables the simultaneous measurement of particle size, velocity, and concentration. Particle image velocimetry (PIV) is a nonintrusive optical measurement technique using a laser light sheet and a CCD camera to investigate flow velocity structures. PIV enables the measurement of instantaneous whole field information of the flow structures, which is not possible with LDA or PDA.

Performing reliable measurements in CFB reactors is very difficult, since high volume fractions of particles prevent proper visual access to the measurement region. This is one of the reasons that numerical methods have become a popular alternative to study the hydrodynamics in circulating fluidized beds. Two theoretical approaches, Eulerian and the discrete particle (Lagrangian) approaches, were proposed to describe the complicated phenomena. Eulerian modeling considers the solid phases as well as the gas phase as continua where the presence of each phase is described by a phase volume fraction. Many resreachers studied the multiphase flow in a riser, in which most adopt the Eulerian method to save computation time. The Eulerian model is able to predict the formation of clusters and describe the time-averaged solid concentration and flux distribution in circulating fluidized beds.[4,5,7,19−27]

The Langrangian (discrete particles) approach includes hard-sphere and soft-sphere models as well as DSMC (direct simulation Monte Carlo) method, in which the particle control volume is considered to move with the fluid.[28−30] Both the interactions between particles and between particles and the gas phase are modeled in this model. Contrary to the two-fluid model, the discrete particle model reveals the motion of individual particles. The DSMC method has relatively large computer memory requirements, so it can only deal with reactors of very small size. Due to the way the collisions are treated in the soft-sphere model, it is restricted to the use of very small time steps, which makes simulations with this model very time-consuming. In this respect, the hard-sphere model seems most suited for simulations with large number of particles. Due to the progress in computer hardware development, the DPM method becomes more and more popular in the computational research of fluidized beds. The advantage of the Lagrangian approach over Eulerian models is the fact that a more detailed model for the particle−particle interactions can be implemented.

In this work the hydrodynamics of gas−solid two-phase turbulent flow in a riser has been studied by detailed experiments using particle image velocimetry and detailed simulations with a 3D discrete particle model (DPM) in a well-defined geometry. The recorded PIV images provide information on the formation, growth, motion, and break-up of clusters.

The gas−solid two-phase flow in the riser has been simulated with a 3D, hard sphere, discrete particle model, applying a subgrid scale (SGS) model to account for the influence of the gas-phase turbulence using the model recently proposed by Vreman.[31] Simulations were performed with a fixed solids influx at the bottom, which allowed investigation of the developing flow regime. The movement and patterns of the clusters and the corresponding mean and rms particle velocities obtained from the simulations for different superficial gas velocities and solids fluxes are compared with the experimental findings.

* To whom correspondence should be addressed. Tel.: +31-53-489 4138. Fax: +31-53-489 2882. E-mail: N.G.Deen@utwente.nl.
[†] University of Twente.
[‡] Harbin Institute of Technology.

10.1021/ie8015285 CCC: $40.75
Published on Web 04/30/2009

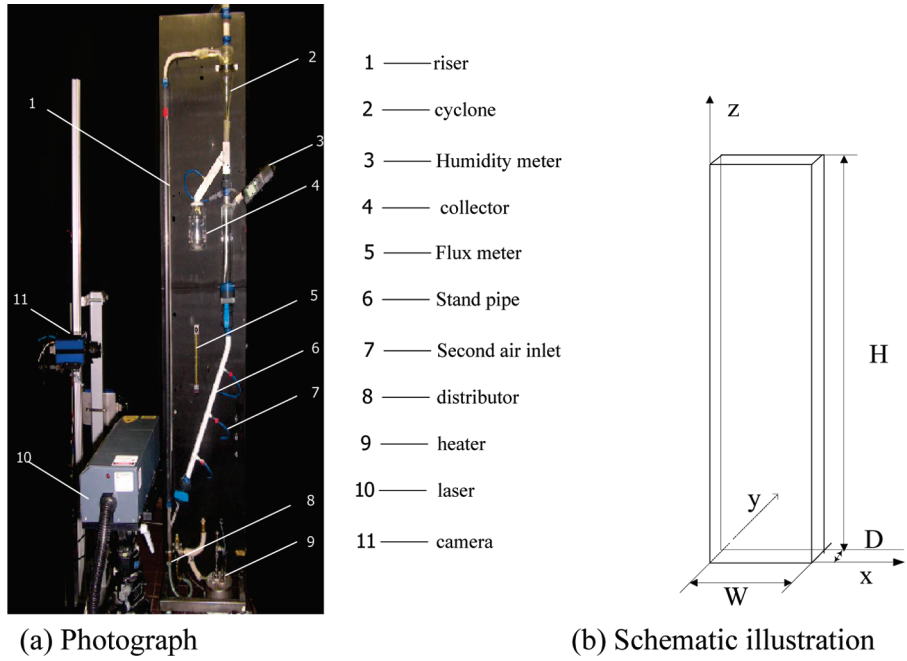

Figure 1. Photograph and schematic illustration of the circulating fluidized bed.

Table 1. Details of the PIV Experimental Setup

camera	Image Pro HS
camera frame rate	800 Hz
pixel pitch	12 μm
camera resolution	1280 × 581 pixels^2
particle−particle collision	
normal restitution	0.97 ± 0.01
friction	0.10 ± 0.01
tangential restitution	0.33 ± 0.01
particle-wall collision	
normal restitution	0.97 ± 0.01
friction	0.10 ± 0.01
tangential restitution	0.33 ± 0.01

2. Experimental Method

2.1. Experimental Setup. In a pseudo two-dimensional circulating fluidized bed constructed of lexane ($W \times D \times H$ = 0.05 m × 1.5 m × 0.015 m) spherical glass beads with a density of 2500 kg/m^3, an average diameter of 335 μm (250−420 μm), and an approximate shape factor of 1.0 were fluidized with air at a superficial gas velocity of 2.00 and 2.30 m/s. The air was humidified up to a relative humidity of 40−60%.

A photograph and a schematic illustration of the experimental setup used in our work are shown in Figure 1a and 1b, respectively. The setup is mainly composed of a riser, gas-particle separation system, and recirculating system.

Experiments have been carried out in this setup focusing on the riser. The bed was illuminated by a laser sheet generated by a pulsed Nd:YAG laser. Images of the bed were recorded at various heights with the use of a high-speed digital camera. Further details of the experimental setup are listed in Table 1.

2.2. Particle Velocity Measurements. Particle image velocimetry (PIV) is a nonintrusive technique for the measurement of an instantaneous velocity field in one plane of a flow. In traditional PIV the flow is visualized by seeding it with small tracer particles that perfectly follow the flow. In gas-particle flows, the discrete particles can readily be distinguished, so no additional tracer particles are needed to visualize the particle movement. The flow in the middle of the bed is illuminated with the use of a laser light sheet. A CCD camera is used to record images of the particles in the illuminated plane. Two subsequent images of the flow, separated by a short time delay, Δt, are divided into small interrogation areas. Cross-correlation analysis is used to determine the volume-averaged displacement, $\mathbf{s}_p(\mathbf{x},t)$, of the particle images between the interrogation areas in the first and second image. The cross-correlation analysis yields a dominant correlation peak embedded in a background of noise peaks, where the location of the tallest peak corresponds to the local average particle displacement. The average particle velocity is then straightforwardly calculated from the displacement vector and the time delay between the two images.

It is difficult to get good quality images for PIV analysis in circulating fluidized beds with increasing particle volume fractions, because the laser cannot penetrate dense zones of particles. Through visual observation, we noted that the right half-part of the riser was well illuminated. For this reason, only results for the right half of the bed are shown in this paper. In the interpretation of the PIV data, one should be aware that the determined velocity vectors represent instantaneous locally *volume-averaged* velocities, which does not take into account the local particle number density that is unknown. Arithmetically time averaging the experimentally obtained velocities yields a different result than the particle number weighted time average, which is typically used in modeling techniques. When the particle volume fraction is uniform, the time average obtained from PIV will correspond to the particle number weighted time average. However, in the case of risers, the particle volume fraction is not uniformly distributed, which complicates the interpretation of the PIV results.

3. Numerical Method

3.1. Description of the Gas Phase. The gas flow is modeled by the volume-averaged Navier−Stokes equations:

$$\frac{\partial(\varepsilon_g \rho_g)}{\partial t} + \nabla(\varepsilon_g \rho_g \mathbf{u}_g) = 0 \tag{1}$$

$$\frac{\partial(\varepsilon_g \rho_g \mathbf{u}_g)}{\partial t} + \nabla(\varepsilon_g \rho_g \mathbf{u}_g \mathbf{u}_g) = -\varepsilon_g \nabla P - \mathbf{S}_p - \nabla(\varepsilon_g \tau_g) + \varepsilon_g \rho_g \mathbf{g} \tag{2}$$

Here, ε_g is the porosity, and ρ_g, $\mathbf{u}_g$, $\boldsymbol{\tau}_g$ and P respectively are the density, velocity, viscous stress tensor and pressure of the gas phase, respectively. The source term $\mathbf{S}_p$ is defined as:

$$\mathbf{S}_p = \frac{1}{V}\int \sum_{a=0}^{N_{part}} \frac{\beta V_a}{1-\varepsilon_g}(\mathbf{u}_g - \mathbf{v}_a)\delta(\mathbf{r} - \mathbf{r}_a)\mathrm{d}V \tag{3}$$

Here V is the volume of the fluid cell, V_a the volume of particle, $\mathbf{v}_a$ the particle velocity, and N_{part} the number of particles. The distribution-function δ distributes the reaction force of the particles exerted on the gas phase to the velocity nodes on the (staggered) Eulerian grid. To calculate the interphase momentum exchange coefficient β we employed the well-known Ergun[32] equation for porosities lower than 0.8 and the Wen and Yu[33] correlation for porosities higher than 0.8.[34]

$$\beta = \begin{cases} 150\dfrac{\mu_g \varepsilon_s^2}{\varepsilon_g^2 d_p^2} + 1.75\dfrac{\rho_g \varepsilon_s}{\varepsilon_g d_p}|\mathbf{u}_g - \mathbf{v}_a| \forall \varepsilon_g \le 0.8 \\ \dfrac{3C_d \varepsilon_s \varepsilon_g \rho_g |\mathbf{u}_g - \mathbf{v}_a|}{4d_p}\varepsilon_g^{-2.65} \forall \varepsilon_g > 0.8 \end{cases} \tag{4}$$

with

$$Re_p = \frac{\rho_g |\mathbf{u}_g - \mathbf{v}_a| d_p}{\mu_g} \tag{5}$$

$$C_d = \begin{cases} \dfrac{24}{Re_p}(1 + 1.15Re_p^{0.687}) \forall Re_p < 1000 \\ 0.44 \forall Re_p \ge 1000 \end{cases} \tag{6}$$

where Re_p, d_p, and $\mathbf{v}_a$ are respectively the particle Reynolds number, diameter, and velocity. ε_s and C_d are the local solids volume fraction and the drag coefficient, respectively.

The gas-phase stress tensor in eq 2 is given by:

$$\tau_g = -\mu_{g,eff}((\nabla \mathbf{u}_g) + (\nabla \mathbf{u}_g)^T - \frac{2}{3}\mathbf{I}(\nabla \mathbf{u}_g)) \tag{7}$$

where the eddy viscosity of the gas is calculated by the SGS model of Vreman:[31]

$$\mu_{g,eff} = c\rho_g \sqrt{\frac{B_\beta}{\alpha_{ij}\alpha_{ij}}} \tag{8}$$

with

$$\alpha_{ij} = \frac{\partial u_{g,j}}{\partial x_i} \tag{9}$$

$$\beta_{ij} = \Delta_m^2 \alpha_{mi}\alpha_{mj} \tag{10}$$

$$B_\beta = \beta_{11}\beta_{22} - \beta_{12}^2 + \beta_{11}\beta_{33} - \beta_{13}^2 + \beta_{22}\beta_{33} - \beta_{23}^2 \tag{11}$$

Here c and Δ_m are respectively a model constant and the local filter width, which will be explained later. Note that the index m in eq 10 indicates a summation over all three coordinate directions. The symbol α stands for the (3 × 3) matrix of derivatives of the filtered velocity $\mathbf{u}_g$. We define that if $\|\alpha_{ij}\alpha_{ij}\| = 0$, then $\mu_{g,eff} = 0$ (where $\|.\|$ is the norm).

The Smagorinsky model is given by:

$$\mu_{g,eff} = \rho_g (C_s \Delta)^2 \|S_{ij}S_{ij}\| \tag{12}$$

where $S_{ij} = (1/2)(\partial \mathbf{u}_j/\partial x_i) + (1/2)(\partial \mathbf{u}_i/\partial x_j)$ is the characteristic filtered strain rate. The model constant c is related to the Smagorinsky constant C_s by $c \approx 2.5C_s^2$. In our simulation we let $C_s = 0.1$ (i.e., $c = 0.025$). Both turbulence models can be implemented in the DPM straightforwardly, since it only requires the local filter width and the first-order derivatives of the velocity field. The gas-phase equations are solved numerically with a finite differencing technique, in which a staggered grid was employed to ensure numerical stability.

Table 2. Parameters Used in the Base Case

parameter	value (units)
particle diameter, d_p	335 (μm)
solid flux, G_s	5, 10, and 20 (kg/m^2 s)
particle density, ρ_p	2500 (kg/m^3)
normal restitution coefficient, e_n	0.97 (−)
tangential restitution coefficient, β_0	0.33 (−)
friction coefficient, μ	0.10 (−)
time step, Δt	5×10^{-5} (s)
channel width, W	0.05 (m)
channel depth, D	0.015 (m)
channel height, H	0.30 (m)
CFD grid number, N_x	25 (−)
CFD grid number, N_y	10 (−)
CFD grid number, N_z	60 (−)
shear viscosity of gas, μ_g	1.8×10^{-5} (Pa s)
gas temperature, T	313 K
pressure, P	1.2×10^5 (P s)
superficial gas velocity, u_{sp}	2.0 and 2.3 (m/s)
particle terminal velocity, u_t	2.7 (m/s)
initial number of particles, N_p	168000 (−)

3.2. Description of the Solid Phase. The hard-sphere discrete particle model (DPM) used in this work was originally developed by Hoomans et al.[35] In the DPM the particles are assumed to be rigid spheres, and collisions among particles are treated as binary, instantaneous, impulsive events, details of which can be found in the work of Hoomans et al.[35] and Deen et al.[36]

The velocity of every individual particle can be calculated from Newton's second law, containing forces due to the pressure gradient, drag, and gravitation:

$$m_a \frac{\mathrm{d}^2 \mathbf{r}_a}{\mathrm{d}t^2} = \frac{V_a \beta}{1-\varepsilon}(\mathbf{u} - \mathbf{v}_a) - V_a \nabla P + m_a \mathbf{g} \tag{13}$$

$$I_a \Omega_a = I_a \frac{\mathrm{d}\omega_a}{\mathrm{d}t} = \mathbf{T}_a \tag{14}$$

Here, m_a is the mass of the particle, $\mathbf{T}_a$ the torque, I_a the moment of inertia, $\boldsymbol{\Omega}_a$ the rotational acceleration, and $\boldsymbol{\omega}_a$ the rotational velocity.

3.3. Initial and Boundary Conditions. A sketch of the fluidized bed riser used in this study is shown in Figure 1. The simulations are carried out only for the central part of the riser section without considering inlet and exit effects. Particles are introduced into the bed with a constant solid flux through the bottom of the bed. All particles are redistributed in the course of the simulation due to the forces acting on them. Gas is injected at the bottom of the riser. A no-slip condition is used for the gas phase at the walls. A pressure boundary condition is used for the gas phase at the top of the bed. Most of the physical parameters are chosen to correspond with the experimental settings. A smaller height of the channel was selected for the simulations compared to the experimental setup to decrease the computation times and the initial total number of particles was reduced accordingly. The simulation settings are summarized in Table 2. The simulation was run for 10 s and time averages were calculated during the last 5 s.

The applied numerical grid was selected in such way that all relevant structures are resolved, while ensuring that the particle volumes are significantly smaller than the volume of a grid cell. The simulations presented in this work have a similar degree of accuracy as the work of Vreman et al.,[37] who uses similar

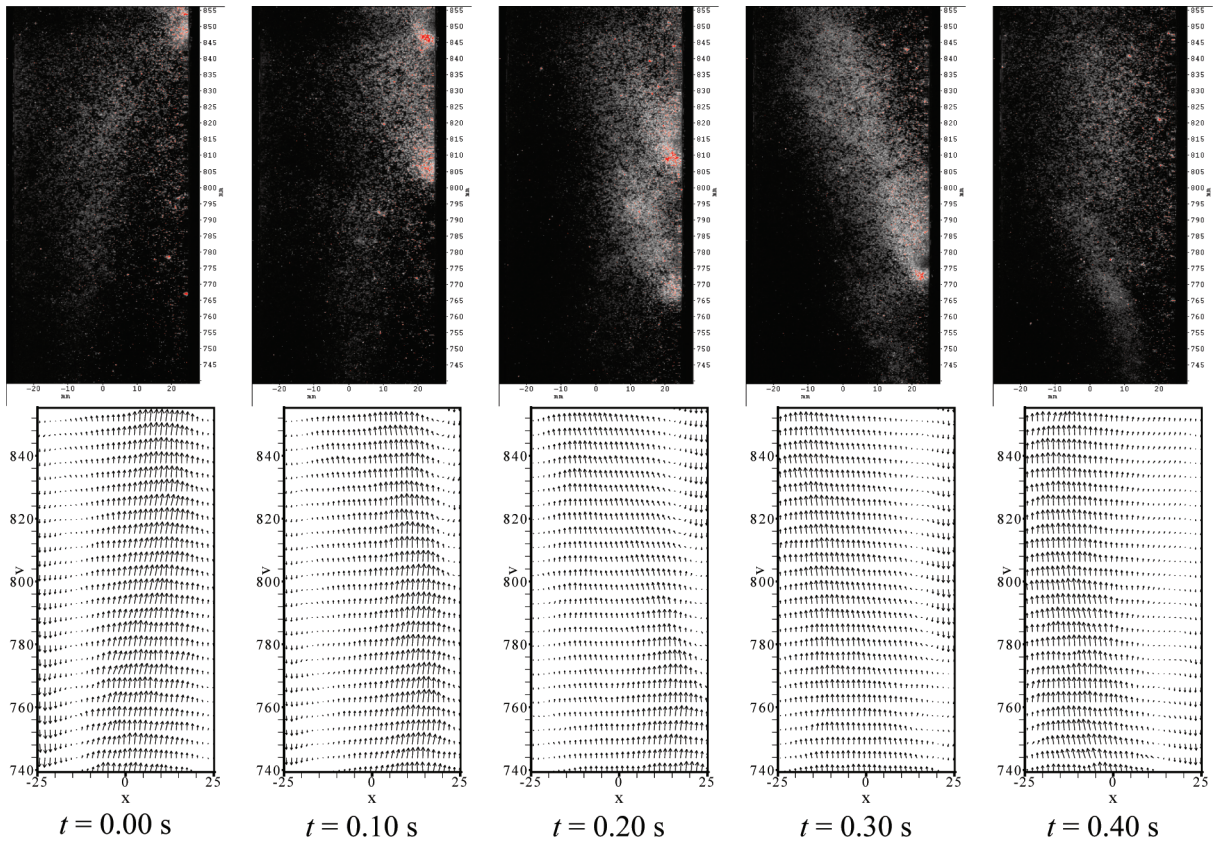

Figure 2. Snapshots of the instantaneous particle positions (top) and corresponding particle velocity fields (bottom) at a superficial gas velocity of 2.3 m/s ($z = 0.740-0.855$, $G_s = 10$ kg/m^2 s).

simulation conditions and who has argued that the grid is sufficiently fine. This implies that a (very costly) grid sensitivity study is not necessary.

4. Results

Particle image velocimetry measurements were performed in the riser for a period of 50 s. Figure 2 shows recorded images and associated velocity fields that were obtained at a solid flux of 10 kg/m^2 s at superficial gas velocity of 2.3 m/s. In this figure, the movement of the clusters can very clearly be observed. The clusters move downward fast along the right wall.

It can also be observed that the particles move upward in the center of the bed, while particles move down in the proximity of the wall. When a cluster is passing by, the particles are dragged down at a higher velocity. This implies that the clusters are too heavy to be dragged by the gas phase and change the flow pattern in the riser. Combined with Figure 4 it can be easily seen that a cluster is followed by a wake, in which particles move downward quickly.

Figures 3 and 4 respectively show the average particle velocity field and corresponding velocity profiles at a solid flux of 10 kg/m^2 s and a superficial gas velocity of 2.3 m/s. It is observed from these figures that the particles move upward in the bed center and move downward closer to the wall. The particle velocity is almost symmetrical and nearly the same along the bed height above $z = 0.8$ m, indicating that the flow is fully developed. The flow for the height of 0.55 and 0.25 m is still developing flow with the particles accelerating and acquiring more energy.

Figure 5 shows the rms particle velocity distributions for the solid flux of 10 kg/m^2 s and a superficial gas velocity of 2.3 m/s at various bed heights. The horizontal component of the

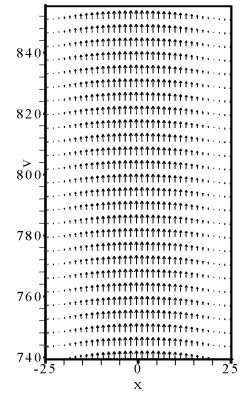

Figure 3. Average particle velocity distribution at superficial gas velocity of 2.3 m/s ($z = 0.740-0.855$, $G_s = 10$ kg/m^2 s).

rms velocity is larger in the center of the bed and decreases toward the wall. The horizontal rms particle velocities at various bed heights are nearly the same. The vertical rms particle velocities are opposite to the horizontal rms particles velocities, i.e. low in bed center and increasing toward the wall. Close to the wall a slight decrease of the vertical rms particle velocities is observed. It is noted that the vertical velocity fluctuations are considerably larger than the horizontal fluctuations, which is in accordance with the flow direction in the riser.

The local maximum in the vertical velocity fluctuations corresponds to the region containing most of the clusters. In the region close to the wall the fluctuations are dampened by the wall. Furthermore, it is observed that the vertical rms particle velocity is high in the bottom of the bed and decreases with the bed height. When the height of the bed is over 0.8 m the vertical rms particle velocities remain almost constant. As

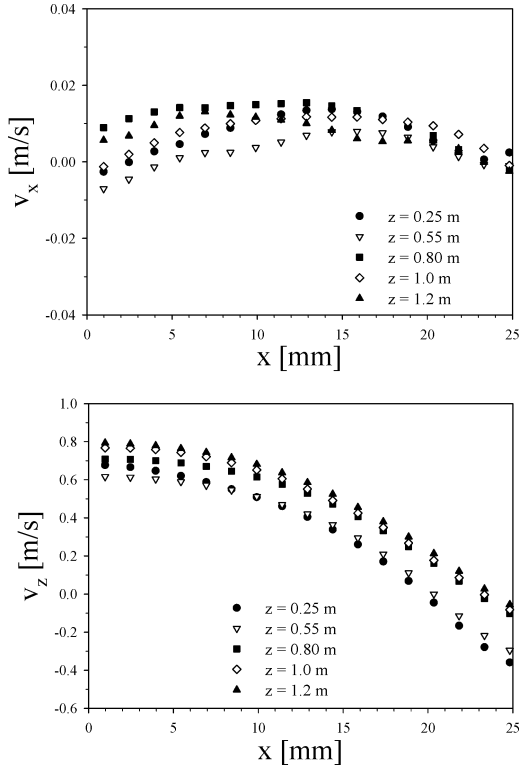

Figure 4. Average particle velocity distributions at superficial gas velocity of 2.3 m/s at various bed heights (G_s = 10 kg/m^2 s).

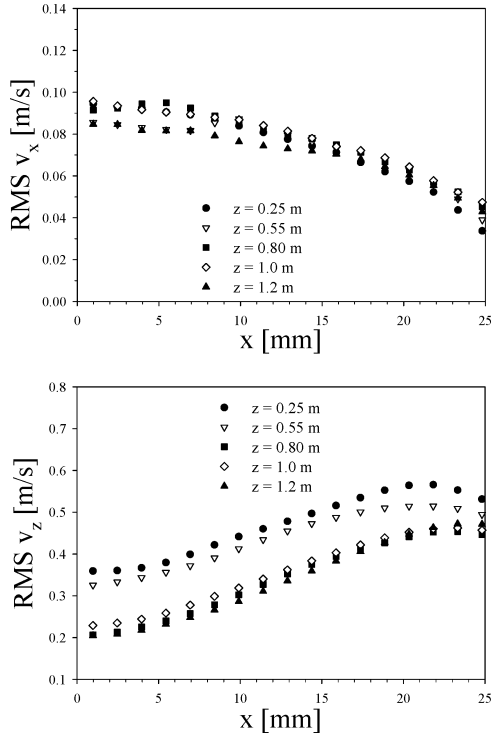

Figure 5. rms particle velocity distributions at superficial gas velocity of 2.3 m/s at various bed heights (G_s = 10 kg/m^2 s).

observed before, the flow is fully developed above bed heights of 0.8 m. Hence, the intensity of fluctuation of the particles remains nearly the same.

Because the superficial gas velocity has an important influence on the flow in a circulating fluidized bed riser, experiments at two different superficial gas velocities were performed in this work. The average particle velocity distribution at superficial

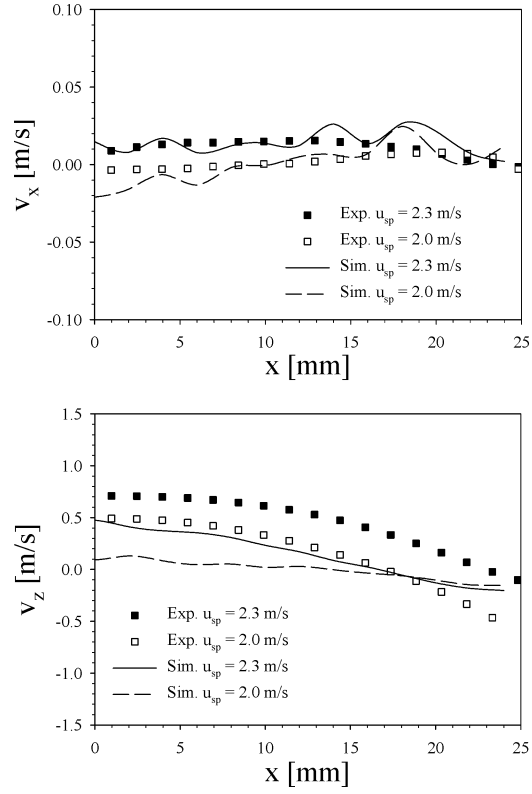

Figure 6. Average particle velocity distributions at various superficial gas velocities (z = 0.80 m, G_s = 10 kg/m^2 s).

gas velocities of 2.0 and 2.3 m/s are shown in Figure 6. The horizontal velocities are small and increase slightly with increasing superficial gas velocity. The vertical velocities are high in the bed center and decrease along the horizontal direction. The vertical particle velocity is largest at a superficial gas velocity of 2.3 m/s. The profiles of the vertical particle velocity have nearly the same shape in both cases, which indicates that the superficial gas velocity has a strong influence on the vertical solid velocity and subsequently on the extent of solids downflow. Numerical results are also shown in Figure 6 with a reasonable agreement to the experimental results. The observed differences may partly be related to the difference in the computation of the average velocities, as discussed in section 2.2. Another reason for the observed discrepancies may be related to systematic errors in the PIV data resulting from difficulties in illuminating dense areas. Finally, the gas-particle drag computed in the DPM may differ from the actual drag. Despite many studies on various drag closures, there is no consensus on what drag model to use.

rms particle velocities at various superficial gas velocities are shown in Figure 7. The horizontal rms particle velocities are small in both cases. The vertical rms velocities for both cases are lower in the bed center and increase with the horizontal direction of the bed to a peak value and then decrease very close to the wall. The vertical rms velocity for low superficial gas velocity changes less with the horizontal direction of the bed than for high superficial gas velocity. The reason for this is that the particles are less influenced by the gas phase at the lower superficial gas velocity.

Figure 8 shows the average particle velocity distributions with various solid fluxes at a superficial gas velocity of 2.3 m/s. The horizontal velocities of particles are small. The vertical velocities of particles are large in the bed center and decrease with the horizontal direction of the bed. The velocity profiles are steeper at higher solid fluxes. The reason for this may be that the cluster

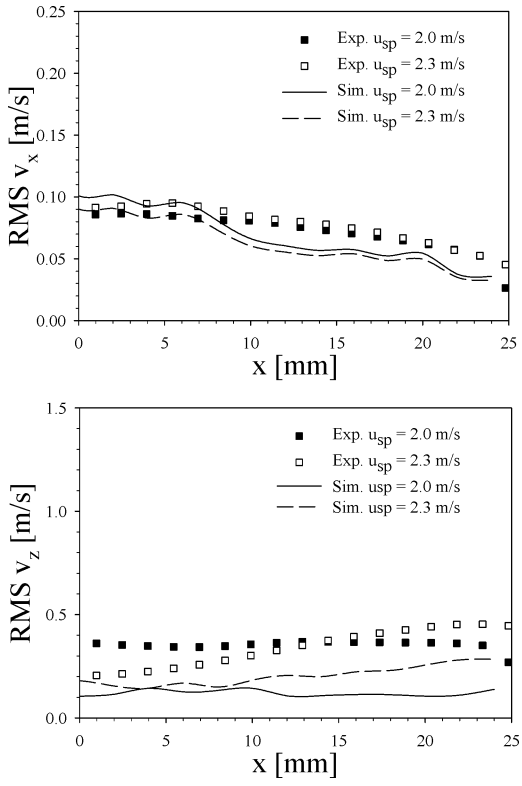

Figure 7. rms particle velocity distributions at various superficial gas velocities (z = 0.80 m, G_s = 10 kg/m^2 s).

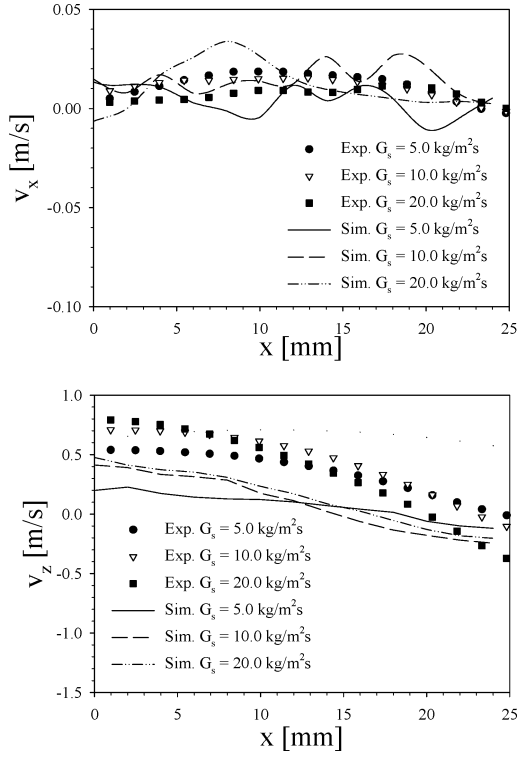

Figure 8. Average particle velocity distributions with various solid fluxes (z = 0.8 m, u_{sp} = 2.3 m/s).

increase in size and weight at higher solid fluxes. Experimental results are compared with numerical result in Figure 8 and are found to be in reasonable agreement, showing the same trends.

rms velocities of particles for various solid fluxes are given in Figure 9. The horizontal rms velocities are nearly the same for all cases. The profiles of the vertical rms velocities show

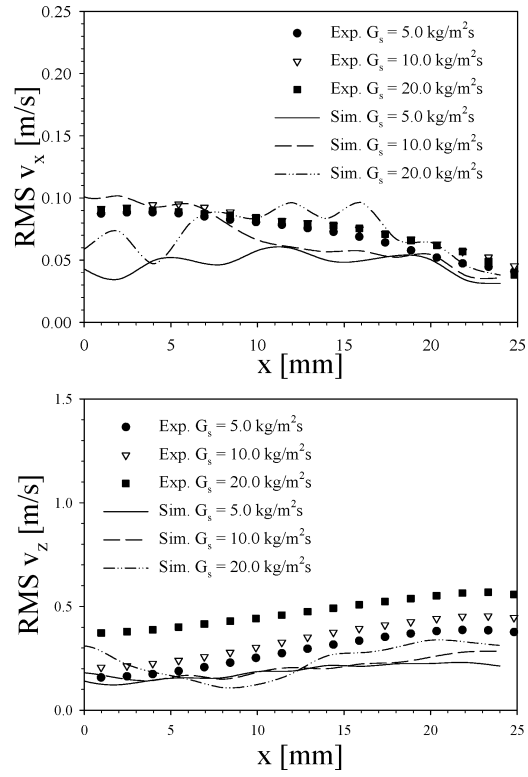

Figure 9. rms particle velocity distributions with various solid fluxes (z = 0.8 m, u_{sp} = 2.3 m/s).

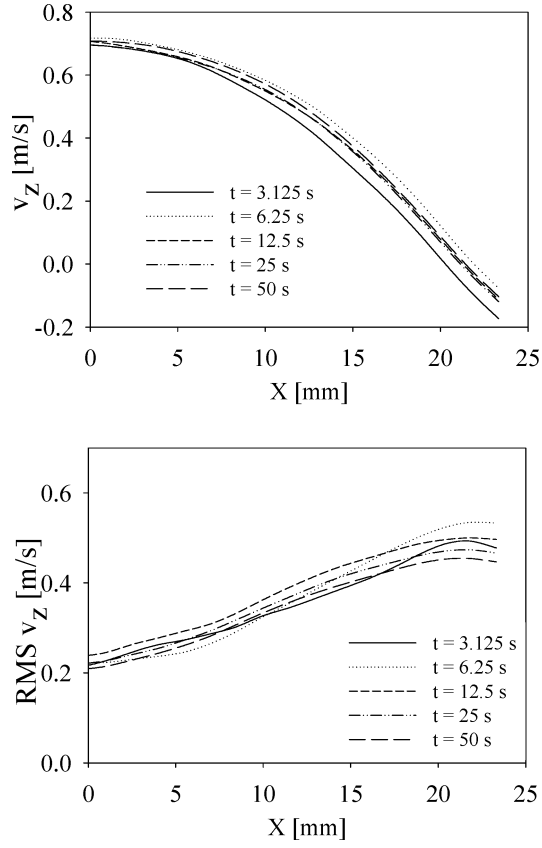

Figure 10. Distribution of mean vertical velocity and vertical rms velocity of particles obtained using various averaging periods of the experimental data (z = 0.8 m, u_{sp} = 2.3 m/s).

considerable differences, which is caused by the clusters characteristics, being bigger and heavier in the case of higher

solid fluxes. Further study on the cluster characteristics is necessary to explain the complex phenomena of the flow in a riser.

Distributions of the mean and rms vertical velocity of the particles employing different averaging periods are presented in Figure 10. We can see that the results for the mean vertical velocity using an averaging period of 3.125 and 6.25 s differ significantly from the other results. For averaging periods longer than 12.5 s the results for the mean and rms velocity change only marginally with increasing averaging periods.

5. Conclusions

In this work the hydrodynamics of gas−solid two-phase turbulent flow in a riser has been studied by detailed experiments using a nonintrusive optical measurement technique, particle image velocimetry (PIV). The gas−solid two-phase flow in the riser has also been simulated with a 3D, hard sphere, discrete particle model, applying a SGS model proposed by Vreman[31] to account for the influence of gas-phase turbulence.

Experimental and numerical results show that from 0.8 m above the bottom distributor plate the core-annulus flow structure has become fully developed. It was found that the superficial gas velocity has a strong influence on the vertical solids velocity and subsequently on the extent of solids downflow. The solids flux has a large effect on the extent of solids downflow but only little influence on the lateral profile of the rms vertical solids velocity. Experimental results in this work indicate that PIV can be an efficient tool for quantitative flow visualization in a flat circulating fluidized bed, even at the relatively high particle volume fractions encountered in these systems.

Acknowledgment

This work was supported by the National Science Foundation through Grant No. 50376013 and NSFC-PetroChina Company Limited under the cooperative project No. 20490200.

Literature Cited

(1) Samuelsberg, A.; Hjertager, B. H. An experimental and numerical study of flow patterns in a circulating fluidized bed reactor. *Int. J. Multiphase Flow* **1996**, *22*, 575.

(2) Zhou, J.; Grace, J. R.; Lim, C. J.; Brereton, C. M. H. Particle velocity profiles in a circulating fluidized bed riser of square cross-section. *Chem. Eng. Sci.* **1995**, *50*, 237.

(3) Hirschberg, B.; Werther, J. Factors affecting solids segregation in circulating fluidized-bed riser. *AIChE J.* **1998**, *44*, 25.

(4) Mathiesen, V.; Solberg, T.; Arastoopour, H.; Hjertager, B. H. Experimental and computational study of multiphase gas/particle flow in a CFB riser. *AIChE J.* **1999**, *45*, 2503.

(5) Mathiesen, V.; Solberg, T.; Hjertager, B. H. An experimental and computational study of multiphase flow behavior in a circulating fluidized bed. *Int. J. Multiphase Flow* **2000**, *26*, 387.

(6) Sharma, A. K.; Tuzla, K.; Matsen, J.; Chen, J. C. Parametric effects of particle size and gas velocity on cluster characteristics in fast fluidized beds. *Powder Technol.* **2000**, *111*, 114.

(7) Neri, A.; Gidaspow, D. Riser hydrodynamics: simulation using kinetic theory. *AIChE J.* **2000**, *46*, 52.

(8) Zhou, H.; Lu, J.; Lin, L. Turbulence structure of the solid phase in transition region of a circulating fluidized bed. *Chem. Eng. Sci.* **2000**, *55*, 839.

(9) Parssinen, J. H.; Zhu, J. X. Axial and radial solids distribution in a long and high-flux CFB riser. *AIChE J.* **2001**, *47*, 2197.

(10) Zhang, H.; Huang, W. X.; Zhu, J. X. Gas-solid flow behavior: CFB riser vs. downer. *AIChE J.* **2001**, *47*, 2000.

(11) Manyele, S. V.; Parssinen, J. H.; Zhu, J. X. Characterizing particle aggregates in a high-density and high-flux CFB riser. Chem. *Eng. J.* **2002**, *88*, 151.

(12) Fan, Y.; Ye, S.; Chao, Z.; Lu, C.; Sun, G.; Shi, M. Gas-solid two-phase flow in FCC riser. *AIChE J.* **2002**, *48*, 1869.

(13) Harris, A. T.; Davidson, J. F.; Thorpe, R. B. Influence of exit geometry in circulating fluidized-bed risers. *AIChE J.* **2003**, *49*, 52.

(14) Kim, S. W.; Kirbas, G.; Bi, H.; Lim, C. J.; Grace, J. R. Flow structure and thickness of annular downflow layer in a circulating fluidized bed riser. *Powder Technol.* **2004**, *142*, 48.

(15) Li, H.; Tong, H. Multi-scale fluidization of Ultrafine powders in a fast-bed-riser/conical-dipleg CFB loop. *Chem. Eng. Sci.* **2004**, *59*, 1897.

(16) Breault, R. W.; Ludlow, C. J.; Yue, P. C. Cluster particle number and granular temperature for cork particles at the wall in the riser of a CFB. *Powder Technol.* **2005**, *149*, 68.

(17) Wang, X.; Gao, S.; Xu, Y.; Zhang, J. Gas-solid flow patterns in a novel dual-loop FCC riser. *Powder Technol.* **2005**, *152*, 90.

(18) Bhusarapu, S.; Al-Dahhan, M. H.; Dudukovic, M. P. Solids flow mapping in a gas-solid riser: Mean holdup and velocity fields. *Powder Technol.* **2006**, *163*, 98.

(19) Sinclair, J. L.; Jackson, R. Gas-particle flow in a vertical pipe with particle-particle interactions. *AIChE J.* **1989**, *35*, 1473.

(20) Pita, J. A.; Sundareasan, S. Gas-solids flow in vertical tubes. *AIChE J.* **1992**, *37*, 1009.

(21) Nieuwland, J. J.; Van Sint Annaland, M.; Kuipers, J. A. M.; Van Swaaij, W. P. M. Hydrodynamic modeling of gas-particle flows in riser reactors. *AIChE J.* **1996**, *42*, 1569.

(22) Hrenya, C. M.; Sinclair, J. L. Effects of particle-particle turbulence in gas-solids flows. *AIChE J.* **1997**, *43*, 853.

(23) Samuelsberg, A.; Hjertager, B. H. Computational modeling of gas-particle flow in a riser. *AIChE J.* **1996**, *42*, 1536.

(24) Dasgupta, S.; Jackson, R.; Sundaresan, S. Gas-particle flow in vertical pipes with high mass loading of particles. *Powder Technol.* **1998**, *96*, 6.

(25) Benyahia, S.; Arastoopour, H.; Knowlton, T. M.; Massah, H. Simulation of particles and gas flow behavior in the riser section of a circulating fluidized bed using the kinetic theory approach for the particulate phase. *Powder Technol.* **2000**, *112*, 24.

(26) Huilin, L.; Gidaspow, D. Hydrodynamics of binary fluidization in a riser: CFD simulation using two granular temperatures. *Chem. Eng. Sci.* **2003**, *58*, 3777.

(27) Wang, S.; Liu, H.; Lu, H.; Liu, W.; Jiamin, D.; Li, W. Flow behavior of clusters in a riser simulated by direct simulation Monte Carlo method. *Chem. Eng. J.* **2005**, *106*, 197.

(28) Tsuji, Y.; Tanaka, T.; Yonemura, S. Cluster patterns in circulating fluidized beds predicted by numerical simulation (discrete particle model versus two-fluid model). *Powder Technol.* **1998**, *95*, 254.

(29) Helland, E.; Occelli, R.; Tadrist, L. Numerical study of cluster formation in a gas-particle circulating fluidized bed. *Powder Technol.* **2000**, *110*, 210.

(30) Sun, Q.; Lu, H.; Liu, W.; He, Y.; Yang, L.; Gidaspow, D. Simulation and experiment of segregating/mixing of rice husk-sand mixture in a bubbling fluidized bed. *Fuel* **2005**, *84*, 1739.

(31) Vreman, A. W. An Eddy-viscosity Subgrid-scale Model for Turbulent Shear Flow: Algebraic Theory and Applications. *Phys. Fluids* **2004**, *16*, 3670.

(32) Ergun, S. Fluid flow through packed columns. *Chem. Eng. Proc.* **1952**, *48*, 89.

(33) Wen, C. Y.; Yu, Y. H. Mechanics of fluidization. *AIChE Ser.* **1966**, *62*, 100.

(34) Gidaspow, D. *Multiphase Flow and Fluidization. Continuum and Kinetic Theory Description*; Academic Press: New York, 1994.

(35) Hoomans, B. P. B.; Kuipers, J. A. M.; Briels, W. J.; Van Swaaij, W. P. M. Discrete particle simulation of bubble and slug formation in a two-dimensional gas-fluidised bed: A hard-sphere approach. *Chem. Eng. Sci.* **1996**, *51*, 99.

(36) Deen, N. G.; Van Sint Annaland, M.; Van der Hoef, M. A.; Kuipers, J. A. M. Review of discrete particle modeling of fluidized beds. *Chem. Eng. Sci.* **2007**, *62*, 28.

(37) Vreman, B.; Geurts, B. J.; Deen, N. G.; Kuipers, J. A. M.; Kuerten, J. G. M. Two- and Four-Way Coupled Euler-Lagrangian Large-Eddy Simulation of Turbulent Particle-Laden Channel Flow. *Flow Turbul. Combust.* **2009**, *82*, 47.

Received for review October 9, 2008
Revised manuscript received April 4, 2009
Accepted April 6, 2009

IE8015285